

文章编号:1009-9603(2018)06-0063-08

DOI:10.13673/j.cnki.cn37-1359/te.2018.06.010

CO₂驱三区复合油藏水平井压力动态分析

姜瑞忠¹,张海涛¹,张 伟¹,陈冠中^{2,3},林春阳^{2,3},原建伟¹

(1. 中国石油大学(华东)石油工程学院,山东 青岛 266580; 2. 海洋石油高效开发国家重点实验室,北京 100028; 3. 中海油研究总院,北京 100028)

摘要:为了给油藏水平井CO₂驱开发提供理论依据,建立CO₂驱三区复合水平井模型,通过拉普拉斯变换、正交变换和数值反演等一系列数学物理方法,求解出解析解。根据流动形态特征,将试井曲线划分为9个阶段,分别是井筒储集阶段、表皮效应阶段、早期径向流阶段、线性流阶段、CO₂区平面径向流阶段、CO₂区向过渡区转移阶段、过渡区径向流阶段、过渡区向原油区转移阶段和原油区径向流阶段。对模型进行一系列敏感性因素分析,结果表明:CO₂区与过渡区半径越大,井底压差越小,越有利于CO₂注入;储容系数越大,过渡区持续时间越短;井筒储集和表皮系数越小对驱替越有利;流度比越大,过渡区持续时间越长。

关键词:水平井 CO₂驱 三区复合模型 试井曲线 解析解

中图分类号:TE357.45

文献标识码:A

Dynamic pressure analysis of three-zone composite horizontal well in oil reservoirs for CO₂ flooding

JIANG Ruizhong¹,ZHANG Haitao¹,ZHANG Wei¹,CHEN Guanzhong^{2,3},LIN Chunyang^{2,3},YUAN Jianwei¹

(1. School of Petroleum Engineering, China University of Petroleum (East China), Qingdao City, Shandong Province, 266580, China; 2. State Key Laboratory of Offshore Oil Exploitation, Beijing City, 100028, China; 3. China National Offshore Oil Corporation, Beijing City, 100028, China)

Abstract: In order to provide a theoretical basis for the development of CO₂ flooding in horizontal wells in oil reservoirs, a three-zone composite horizontal well model for CO₂ flooding was proposed. A series of mathematical and physical methods such as Laplace transformation, orthogonal transformation, and numerical inversion were adopted to solve this model. According to the pressure response characteristics, the well testing curves were divided into nine stages including the wellbore storage stage, skin effect stage, early radial flow stage, linear flow stage, plane radial flow of CO₂ zone, transfer stage of CO₂ zone to transition zone, the radial flow in transition zone, the transfer stage from the transition zone to the crude oil zone and the radial flow in the crude oil zone. Sensitivity analysis was conducted on several influential factors, and results show that when the radius of the CO₂ zone and transition zone become larger, the dimensionless bottomhole pressure difference will decrease, which is favorable for CO₂ injection; the larger the storability ratio is, the shorter the flow time in the transition zone will be; the decrease of the wellbore storage coefficient and skin factor is more favorable for the displacement process; the greater the mobility ratio is, the longer the flow time in the transition zone will last.

Key words: horizontal well; CO₂ flooding; three-zone composite model; well testing curve; analytical solution

随着传统能源产量的减少,非常规能源的开采比重越来越大,目前,开采最为普遍的就是低渗透油藏。低渗透油藏具有低孔低渗透特征,其水驱效

果不明显,采收率较低。CO₂驱代替水驱,降低了原油界面张力和原油粘度等,使原油采收率得到大幅提高^[1-2]的同时解决了部分温室气体的排放问题,在

收稿日期:2018-07-26。

作者简介:姜瑞忠(1964—),男,江苏溧阳人,教授,博士,从事气田开发研究与教学工作。联系电话:18678967281, E-mail: jrzhong@126.com。

基金项目:国家科技重大专项“厚层非均质性气藏产能评价及预测技术研究”(2016ZX05027-004-004),中海石油(中国)有限公司科技项目“分级组合区块深部调剖技术扩大试验研究”(YXKY-2016-ZY-02)。

多年应用CO₂驱的北美地区,CO₂的年利用量高达50×10⁶ t/a^[3-4],CO₂驱可以增加25×10⁴ bbl原油^[5-7],由此可见,CO₂驱具有广阔的应用前景,有必要研究CO₂驱替模型^[8-11]。

试井是了解地下油藏和流体性质的重要手段。目前,已对CO₂驱试井开展了一些研究,TANG等通过分析CO₂注入井压力资料,发现压力响应表现出三区复合油藏特性,即CO₂区、CO₂-原油过渡区(简称过渡区)及未波及原油区(简称原油区)^[12],但未基于这种现象建立数学模型来阐释CO₂驱替过程中压力传播规律;AMBASTHA等建立了基本的三区复合油藏模型,该模型具有低流度比和拟稳定区,被认为是更准确的瞬态压力分析模型^[13];SU等研究了CO₂驱直井的三区复合瞬时压力模型,将储层中流体的流动状态分为7个阶段,讨论了部分流动因素的影响^[3]。

目前,中外还没有针对水平井的CO₂驱试井模型,基于以往学者的研究,建立水平井CO₂驱三区复合模型。考虑井筒储集效应和表皮效应,通过拉普拉斯变换、正交变换和数值反演等一系列数学物理方法,求解出解析解,并根据CO₂驱试井曲线的变化特征及其影响因素,给出9种流动状态,并进行较为具体和深入的分析。

1 物理和数学模型

1.1 模型建立

1.1.1 物理模型

基于CO₂驱油机理,建立CO₂驱油模型,通过比较油藏压力和最小混相压力,将CO₂驱油类型分为混相驱和非混相驱^[14-15],这2类CO₂驱油的混合特性都与组分饱和度、温度和初始粘度等无关^[16-17]。由于CO₂性质稳定,CO₂注入的试井模型应建立在多区域假设的基础上^[3]。

CO₂与原油之间的混溶是通过多接触混相驱实现的,其特征是CO₂与原油之间的组分转移,随着CO₂溶于油中,油体积膨胀,粘度降低,在混溶条件下,CO₂相完全消失,CO₂-油的毛管压力和界面张力也随之消失^[17-19]。因此,近井附近可以被视为纯CO₂区,对于仍处于原始状态的流体,可视为纯油区。在这2个区域的中间,应重新定义中间区域,而不是简单地将其处理为CO₂区和纯油区,忽略中间区域^[20-22]。

根据CO₂驱替过程中油藏流体的不同性质,确定模型为:①CO₂区,即纯CO₂的近井区域(一区)。

②过渡区,即在混溶/不混溶条件下,CO₂和油的混合物的中间区域(二区)。③原油区,即处于原始状态的外部区域(三区)。

建立CO₂驱三区复合水平井物理模型如图1所示,三区的半径分别为r₁,r₂和r₃(r₃→∞时为无限大油藏)。

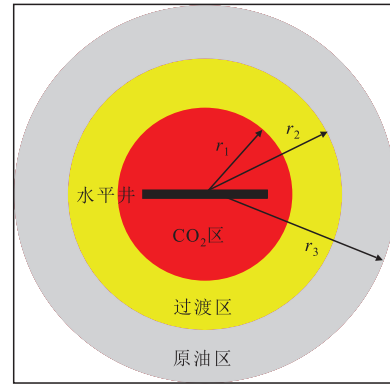


图1 CO₂驱三区复合水平井物理模型示意

Fig.1 Physical modeling of three-zone composite horizontal wells for CO₂ flooding

1.1.2 数学模型

数学模型的假设包括:①储层性质均匀,地层为水平、均质、等厚,规模无限大,上、下有不渗透隔层。②油气藏中油气共存,流动过程等温。③烃类组分分布在油气相中。④忽略吸附效应、重力及毛管压力作用。⑤流体的流动遵循达西定律,忽视扩散效应。⑥CO₂区及原油区内流体流度及储容系数恒定。

定义无因次变量为

$$r_D = \frac{r}{L} \quad (1)$$

$$t_D = \frac{t}{L^2} \eta_1 = \frac{K_{h1} t}{\phi_1 \mu_g C_g L^2} \quad (2)$$

$$q_D = \frac{-q_{sc} \mu_g}{2\pi K_{h1} h p_i} \times \frac{p_{sc} T Z}{p_i T_{sc}} \quad (3)$$

$$\psi_{pD} = \frac{2\pi K_{h1} h [m(p_j) - m(p_i)]}{q_{sc} \mu_g} \quad j = 1, 2, 3 \quad (4)$$

$$C_D = \frac{C}{2\pi \phi_1 C_{11} h L^2} \quad (5)$$

$$M_{12} = \frac{\frac{K_{h1}}{\mu_1}}{\frac{K_{rg} K_{h2}}{\mu_g} + \frac{K_{ro} K_{h2}}{\mu_o}} \quad (6)$$

$$M_{23} = \frac{\frac{K_{rg} K_{h2}}{\mu_g} + \frac{K_{ro} K_{h2}}{\mu_o}}{\frac{K_{h3}}{\mu_o}} \quad (7)$$

$$\omega_{12} = \frac{\eta_1}{\eta_2} \quad (8)$$

$$\omega_{13} = \frac{\eta_1}{\eta_3} \quad (9)$$

$$L_{jD} = \frac{L}{h} \sqrt{\frac{K_{jh}}{K_{jv}}} \quad j=1,2,3 \quad (10)$$

根据无因次变量,得到CO₂区、过渡区和原油区的无因次数学模型分别为

$$\frac{\partial^2 \psi_{1D}}{\partial r_D^2} + \frac{1}{r_D} \frac{\partial \psi_{1D}}{\partial r_D} + L_{1D}^2 \frac{\partial^2 \psi_{1D}}{\partial z_D^2} = \frac{\partial \psi_{1D}}{\partial t_D} \quad 0 < r_D < r_{1D} \quad (11)$$

$$\frac{\partial^2 \psi_{2D}}{\partial r_D^2} + \frac{1}{r_D} \frac{\partial \psi_{2D}}{\partial r_D} + L_{2D}^2 \frac{\partial^2 \psi_{2D}}{\partial z_D^2} = \omega_{12} \frac{\partial \psi_{2D}}{\partial t_D} \quad r_{1D} < r_D < r_{2D} \quad (12)$$

$$\frac{\partial^2 \psi_{3D}}{\partial r_D^2} + \frac{1}{r_D} \frac{\partial \psi_{3D}}{\partial r_D} + L_{3D}^2 \frac{\partial^2 \psi_{3D}}{\partial z_D^2} = \omega_{13} \frac{\partial \psi_{3D}}{\partial t_D} \quad r_{2D} < r_D < \infty \quad (13)$$

内边界条件为

$$\lim_{\varepsilon \rightarrow 0} \int_{z_w - \frac{\varepsilon}{2}}^{z_w + \frac{\varepsilon}{2}} \left(r_D \frac{\partial \psi_{3D}}{\partial r_D} \right) dz_w = -\frac{1}{2} \quad (14)$$

外边界条件为

$$\lim_{r_D \rightarrow \infty} \psi_{3D} = 0 \quad (15)$$

CO₂区与过渡区、过渡区与原油区的交界面条件分别为

$$\begin{cases} r_D = r_{1D} \\ \psi_1 = \psi_2 \\ \frac{\partial \psi_1}{\partial r_D} = \frac{1}{M_{12}} \frac{\partial \psi_2}{\partial r_D} \end{cases} \quad (16)$$

$$\begin{cases} r_D = r_{2D} \\ \psi_2 = \psi_3 \\ \frac{\partial \psi_2}{\partial r_D} = \frac{1}{M_{23}} \frac{\partial \psi_3}{\partial r_D} \end{cases} \quad (17)$$

1.2 模型求解

将无因次数学模型及边界条件进行Laplace变换,得

$$\bar{\psi}_D(s) = \int_0^\infty e^{-st_D} \psi_D(t_D) dt_D \quad (18)$$

得到CO₂区、过渡区、原油区数学模型、内外边界条件、CO₂区和过渡区的交界面条件、过渡区和原油区的交界面条件分别为

$$\frac{\partial^2 \bar{\psi}_{1D}}{\partial r_D^2} + \frac{1}{r_D} \frac{\partial \bar{\psi}_{1D}}{\partial r_D} + L_{1D}^2 \frac{\partial^2 \bar{\psi}_{1D}}{\partial z_D^2} = s \bar{\psi}_{1D} \quad 0 < r_D < r_{1D} \quad (19)$$

$$\frac{\partial^2 \bar{\psi}_{2D}}{\partial r_D^2} + \frac{1}{r_D} \frac{\partial \bar{\psi}_{2D}}{\partial r_D} + L_{2D}^2 \frac{\partial^2 \bar{\psi}_{2D}}{\partial z_D^2} = s \omega_{12} \bar{\psi}_{2D} \quad r_{1D} < r_D < r_{2D} \quad (20)$$

$$\frac{\partial^2 \bar{\psi}_{3D}}{\partial r_D^2} + \frac{1}{r_D} \frac{\partial \bar{\psi}_{3D}}{\partial r_D} + L_{3D}^2 \frac{\partial^2 \bar{\psi}_{3D}}{\partial z_D^2} = s \omega_{13} \bar{\psi}_{3D} \quad r_{2D} < r_D < \infty \quad (21)$$

$$\begin{cases} \lim_{\varepsilon \rightarrow 0} \int_{z_w - \frac{\varepsilon}{2}}^{z_w + \frac{\varepsilon}{2}} \left(r_D \frac{\partial \bar{\psi}_{1D}}{\partial r_D} \right) dz_w = -\frac{1}{2s} \\ \lim_{r_D \rightarrow \infty} \bar{\psi}_{3D} = 0 \end{cases} \quad (22)$$

$$\begin{cases} r_D = r_{1D} \\ \bar{\psi}_1 = \bar{\psi}_2 \\ \frac{\partial \bar{\psi}_1}{\partial r_D} = \frac{1}{M_{12}} \frac{\partial \bar{\psi}_2}{\partial r_D} \end{cases} \quad (23)$$

$$\begin{cases} r_D = r_{2D} \\ \bar{\psi}_2 = \bar{\psi}_3 \\ \frac{\partial \bar{\psi}_2}{\partial r_D} = \frac{1}{M_{23}} \frac{\partial \bar{\psi}_3}{\partial r_D} \end{cases} \quad (24)$$

根据有限余弦积分变换得

$$\bar{\bar{\psi}}_D = \int_0^1 \bar{\psi}_D(r_D, z_D) \cos(n\pi z_D) dz_D \quad (25)$$

进行正交变换得到CO₂区、过渡区、原油区、内外边界条件、CO₂区和过渡区的交界面条件、过渡区和原油区的交界面条件数学模型分别为

$$\frac{\partial^2 \bar{\bar{\psi}}_{1D}}{\partial r_D^2} + \frac{1}{r_D} \frac{\partial \bar{\bar{\psi}}_{1D}}{\partial r_D} = (s + n^2 \pi^2 L_{1D}^2) \bar{\bar{\psi}}_{1D} \quad 0 < r_D < r_{1D} \quad (26)$$

$$\frac{\partial^2 \bar{\bar{\psi}}_{2D}}{\partial r_D^2} + \frac{1}{r_D} \frac{\partial \bar{\bar{\psi}}_{2D}}{\partial r_D} = (s \omega_{12} + n^2 \pi^2 L_{2D}^2) \bar{\bar{\psi}}_{2D} \quad r_{1D} < r_D < r_{2D} \quad (27)$$

$$\frac{\partial^2 \bar{\bar{\psi}}_{3D}}{\partial r_D^2} + \frac{1}{r_D} \frac{\partial \bar{\bar{\psi}}_{3D}}{\partial r_D} = (s \omega_{13} + n^2 \pi^2 L_{3D}^2) \bar{\bar{\psi}}_{3D} \quad r_{2D} < r_D < \infty \quad (28)$$

$$\begin{cases} r_D = r_{1D} \\ \bar{\bar{\psi}}_1 = \bar{\bar{\psi}}_2 \\ \frac{\partial \bar{\bar{\psi}}_1}{\partial r_D} = \frac{1}{M_{12}} \frac{\partial \bar{\bar{\psi}}_2}{\partial r_D} \end{cases} \quad (29)$$

$$\begin{cases} r_D = r_{2D} \\ \bar{\bar{\psi}}_2 = \bar{\bar{\psi}}_3 \\ \frac{\partial \bar{\bar{\psi}}_2}{\partial r_D} = \frac{1}{M_{23}} \frac{\partial \bar{\bar{\psi}}_3}{\partial r_D} \end{cases} \quad (30)$$

$$\begin{cases} \lim_{r_D \rightarrow 0} r_D \frac{\partial \bar{\bar{\psi}}_{1D}}{\partial r_D} = -\frac{\cos(n\pi z_{wD})}{2sL} \\ \lim_{r_D \rightarrow \infty} \bar{\bar{\psi}}_{1D} = 0 \end{cases} \quad (31)$$

得到关于r_D的虚宗量Bessel的函数通解为

$$\bar{\bar{\psi}}_{1D} = A_1 I_0(\sqrt{f_1^n} r_D) + B_1 K_0(\sqrt{f_1^n} r_D) \quad (32)$$

$$\bar{\psi}_{2D} = A_2 I_0(\sqrt{f_2^n} r_D) + B_2 K_0(\sqrt{f_2^n} r_D) \quad (33)$$

$$\bar{\psi}_{3D} = A_3 I_0(\sqrt{f_3^n} r_D) + B_3 K_0(\sqrt{f_3^n} r_D) \quad (34)$$

其中

$$f_1^n = s + n^2 \pi^2 L_{1D}^2 \quad (35)$$

$$f_2^n = s\omega_{12} + n^2 \pi^2 L_{2D}^2 \quad (36)$$

$$f_3^n = s\omega_{13} + n^2 \pi^2 L_{3D}^2 \quad (37)$$

通过外边界条件可得

$$\lim_{r_D \rightarrow \infty} \bar{\psi}_{3D} = \lim_{r_D \rightarrow \infty} [A_3 I_0(\sqrt{f_3^n} r_D) + B_3 K_0(\sqrt{f_3^n} r_D)] = 0 \quad (38)$$

根据 Bessel 方程渐近线关系, 可得 $A_3=0$ 。

通过内边界条件, 得

$$\begin{aligned} \lim_{r_D \rightarrow 0} r_D \frac{\partial \bar{\psi}_{1D}}{\partial r_D} &= \lim_{r_D \rightarrow 0} \left\{ r_D [A_1 I_1(\sqrt{f_1^n} r_D) - B_1 K_1(\sqrt{f_1^n} r_D)] \right\} = \\ &-B_1 \lim_{r_D \rightarrow 0} \left[\sqrt{f_1^n} r_D K_1(\sqrt{f_1^n} r_D) \right] = -\frac{\cos(n\pi z_{wD})}{2sL} \end{aligned} \quad (39)$$

根据 Bessel 方程的性质

$$\lim_{x \rightarrow 0} [xK_1(x)] = 1 \quad (40)$$

得

$$B_1 = \frac{\cos(n\pi z_{wD})}{2sL} \quad (41)$$

定义变量为

$$\begin{cases} a_{11} = I_0(\sqrt{f_1^n} r_{1D}) \\ a_{12} = K_0(\sqrt{f_1^n} r_{1D}) \\ a_{13} = I_0(\sqrt{f_2^n} r_{1D}) \\ a_{14} = K_0(\sqrt{f_2^n} r_{1D}) \end{cases} \quad (42)$$

$$\begin{cases} a_{21} = I_1(\sqrt{f_1^n} r_{1D}) \\ a_{22} = -K_1(\sqrt{f_1^n} r_{1D}) \\ a_{23} = \frac{\sqrt{f_2^n}}{M_{12} \sqrt{f_1^n}} I_1(\sqrt{f_2^n} r_{1D}) \\ a_{24} = -\frac{\sqrt{f_2^n}}{M_{12} \sqrt{f_1^n}} K_1(\sqrt{f_2^n} r_{1D}) \end{cases} \quad (43)$$

$$\begin{cases} a_{31} = I_0(\sqrt{f_2^n} r_{2D}) \\ a_{32} = K_0(\sqrt{f_2^n} r_{2D}) \\ a_{33} = I_0(\sqrt{f_3^n} r_{2D}) \\ a_{34} = K_0(\sqrt{f_3^n} r_{2D}) \end{cases} \quad (44)$$

$$\begin{cases} a_{41} = I_1(\sqrt{f_2^n} r_{2D}) \\ a_{42} = -K_1(\sqrt{f_2^n} r_{2D}) \\ a_{43} = \frac{\sqrt{f_3^n}}{M_{23} \sqrt{f_2^n}} I_1(\sqrt{f_3^n} r_{2D}) \\ a_{44} = -\frac{\sqrt{f_3^n}}{M_{23} \sqrt{f_2^n}} K_1(\sqrt{f_3^n} r_{2D}) \end{cases} \quad (45)$$

将式(32)一式(34)以及式(42)一式(44)代入式(29)和式(30)中得

$$\begin{cases} a_{11}A_1 + a_{12}B_1 = a_{13}A_2 + a_{14}B_2 \\ a_{21}A_1 + a_{22}B_1 = a_{23}A_2 + a_{24}B_2 \\ a_{31}A_2 + a_{32}B_2 = a_{33}A_3 + a_{34}B_3 \\ a_{41}A_2 + a_{42}B_2 = a_{43}A_3 + a_{44}B_3 \end{cases} \quad (46)$$

计算得

$$A_1 = g_2^n B_1 = -g_2^n \frac{\cos(n\pi z_{wD})}{2sL} \quad (47)$$

其中

$$\begin{cases} g_1^n = \frac{a_{31}a_{44} - a_{34}a_{41}}{a_{34}a_{42} - a_{32}a_{44}} \\ g_2^n = \frac{a_{22}(a_{13} + a_{14}g_1^n) - a_{12}(a_{23} + a_{24}g_1^n)}{a_{11}(a_{23} + a_{24}g_1^n) - a_{21}(a_{13} + a_{14}g_1^n)} \end{cases} \quad (48)$$

因此, 根据 A_1 和 B_1 , 求解数学模型得到

$$\begin{aligned} \bar{\psi}_{1D} &= A_1 I_0(\sqrt{f_1^n} r_D) + B_1 K_0(\sqrt{f_1^n} r_D) = \\ &\frac{\cos(n\pi z_{wD})}{2Ls} [g_2^n I_0(\sqrt{f_1^n} r_D) + K_0(\sqrt{f_1^n} r_D)] \end{aligned} \quad (49)$$

应用反余弦变换可得

$$\bar{\xi}_{1D} = C_0 + 2 \sum_{n=1}^{\infty} C_n \cos(n\pi z_D) \quad (50)$$

$$\begin{aligned} \bar{\psi}_{wD} &= \frac{1}{2Ls} [g_2^0 I_0(\sqrt{f_1^0} r_D) + K_0(\sqrt{f_1^0} r_D)] + \\ &\frac{1}{Ls} \sum_{n=1}^{\infty} \left\{ \cos(n\pi z_{wD}) \cos(n\pi z_D) \times \right. \\ &\left. [g_2^n I_0(\sqrt{f_1^n} r_D) + K_0(\sqrt{f_1^n} r_D)] \right\} \end{aligned} \quad (51)$$

点源沿着水平井方向从 $-L$ 到 L 积分, 可以得到整个水平井在储层中引起的压力响应, 作为复合储层中心的线源。当水平井完全位于内部区域时, 拉普拉斯域的井筒压力分布为

$$\begin{aligned} \bar{\psi}_{wD0} &= \int_{-1}^1 \frac{1}{2s} [g_2^0 I_0(\sqrt{f_1^0} r_D) + K_0(\sqrt{f_1^0} r_D)] + \\ &\int_{-1}^1 \frac{1}{s} \sum_{n=1}^{\infty} \left\{ \cos(n\pi z_{wD}) \cos(n\pi z_D) \times \right. \\ &\left. [g_2^n I_0(\sqrt{f_1^n} r_D) + K_0(\sqrt{f_1^n} r_D)] \right\} \end{aligned} \quad (52)$$

其中

$$r_D = \sqrt{(x_D - x_{wD})^2 + (y_D - y_{wD})^2} \quad (53)$$

采用杜哈美原理的方法,考虑井筒储集和表皮效应后的井底压力解为

$$\bar{\psi}_{wD}(s, C_D, S) = \frac{s\bar{\psi}_{wD}(s) + \frac{S}{2L_{1D}}}{s + C_D s^2 \left[s\bar{\psi}_{wD}(s) + \frac{S}{2L_{1D}} \right]} \quad (54)$$

因此,在获得无因次拟压力解后,利用Stehfest数值反演可求得实空间下的井底压力响应,即

$$\psi_{wD}(s) = \frac{1}{s^2} \times \left\{ \psi'_{wD}(1) [1 - e^{-st_D(1)}] + \sum_{i=2}^{n-1} \psi'_{wD}(i) [e^{-st_D(i-1)} - e^{-st_D(i)}] + \psi'_{wD}(n) e^{-st_D(n)} \right\} \quad (55)$$

其中

$$\psi'_{wD}(i) = \frac{\psi_{wD}(i) - \psi_{wD}(i-1)}{t_D(i) - t_D(i-1)} \quad (56)$$

2 CO₂驱试井曲线形态分析

根据求出实空间下的解析解,绘制出2种类型曲线即双对数无因次压力曲线和无因次压力导数曲线,用这2种曲线来描述无限大油藏CO₂驱的流动过程。

2.1 流动形态划分

由压力导数曲线(图2)可见,CO₂驱油藏的渗流过程包括9个阶段:①第1阶段为井筒储集效应主导时期,表征续流段影响。②第2阶段为表皮效应阶段,压力导数曲线在该阶段到达极值后下降。③第3阶段是早期径向流阶段,曲线表现为凹形,这段时间内油在垂直平面内径向流入井眼,将压力波持续传播到顶部/底部边界。④第4阶段是线性流阶段,压力导数曲线表现为斜率为1的直线,受到CO₂区与过渡区流度比、综合储容比的影响。⑤第5阶段为CO₂区平面径向流阶段,与第3阶段相似,曲线

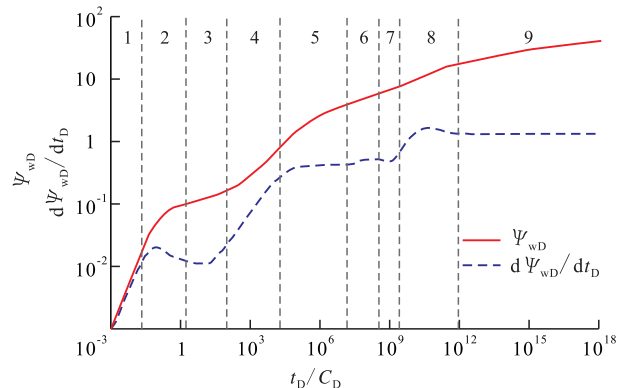


图2 CO₂驱试井流动阶段划分

Fig.2 Division of flow regimes during the CO₂ injection by horizontal wells

上表现为水平。⑥第6阶段是CO₂区向过渡区转移阶段,这个时期压力导数曲线呈略微凸起。⑦第7阶段是过渡区径向流阶段。⑧第8阶段是过渡区向原油区转移阶段,这个时期在压力导数曲线的显著特征是表现为凸起状。⑨第9阶段为原油区径向流阶段,在压力导数曲线上表现为1条水平线。

2.2 参数敏感性分析

2.2.1 弹性储容系数

设置不变参数值分别为: $S=1, Z_{wD}=0.5, M_{12}=1, M_{23}=3, C_D=0.000\ 01, L_{1D}=1, r_{1D}=30, r_{2D}=300, x_D=0.732$ 。

由于每个区域的流体性质差异较大,因此,需要研究各个区域的储容比对曲线的影响。为了直观研究 ω_{12} 和 ω_{13} 的影响,简化图形,定义3组值,分别为 $\omega_{12}=2, \omega_{13}=3; \omega_{12}=4, \omega_{13}=6; \omega_{12}=6, \omega_{13}=9$ 。由弹性储容系数对压力动态的影响(图3)可见, ω_{12} 主要影响CO₂区向过渡区转移阶段的流动形态, ω_{13} 主要影响过渡区向原油区转移阶段的流动形态。随着 ω_{12} 和 ω_{13} 值的增大,压力导数曲线表现为向上移动,过渡区凸形的极值增加,并且可以看出过渡区向原油区转移时间提前,即过渡区持续时间缩短。

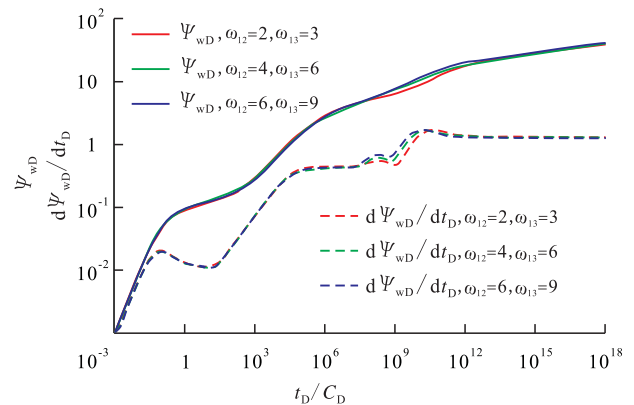


图3 ω_{12} 与 ω_{13} 对压力动态的影响

Fig.3 Effect of ω_{12} and ω_{13} on pressure dynamics

2.2.2 CO₂区与过渡区流度比

设置不变参数值分别为: $S=1, Z_{wD}=0.5, C_D=0.000\ 01, M_{23}=3, \omega_{12}=2, \omega_{13}=3, L_{1D}=1, r_{1D}=30, r_{2D}=300, x_D=0.732$ 。

设置CO₂区与过渡区流度比分别为1,2和2.4。由CO₂区与过渡区流度比对压力动态的影响(图4)可以很容易看出,流度比影响CO₂区向过渡区转移阶段凸形的极值,以及过渡区向原油区转移阶段凸形的极值。随着 M_{12} 逐渐增加,压力导数曲线在第6阶段之后整体上移。考虑到CO₂区中纯CO₂的参数可视为常数,得出流体在过渡区中粘度增加的结论。过渡区流体性质变差,粘度增大。在这种情况下,过渡区径向流的持续时间增加,后一段时间被

推迟。压力曲线在第9阶段斜率不同,表明流度比
对双对数压力曲线形状有影响。

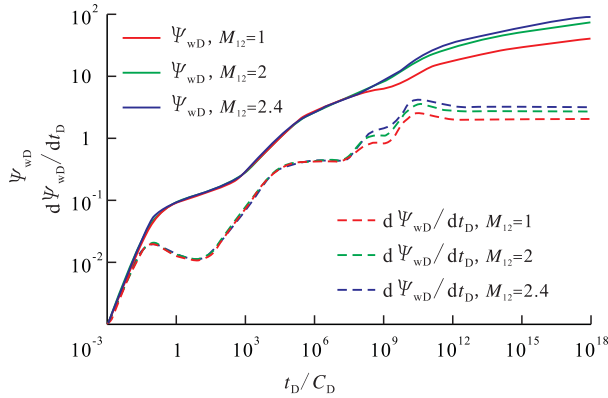


图4 CO₂区与过渡区流度比对压力动态的影响

Fig.4 Influence of mobility ratio of CO₂ region and transition region on pressure dynamics

2.2.3 各区域半径

设置不变参数值分别为: $C_D=0.000\ 01, Z_{wD}=0.5, M_{12}=1, M_{23}=3, \omega_{12}=2, \omega_{13}=3, L_{1D}=1, S=1, x_D=0.732$ 。

在CO₂驱替过程中,由于CO₂不断向过渡区扩散,使得CO₂区无因次半径 r_{1D} 和过渡区无因次半径 r_{2D} 不断增大,假定各区间流度比和储容比恒定,为了简化图形,便于分析,定义3组值,分别为 $r_{1D}=30, r_{2D}=300; r_{1D}=60, r_{2D}=600; r_{1D}=80, r_{2D}=800$ 。由CO₂区和过渡区无因次半径对压力动态的影响(图5)可见,无因次半径主要影响CO₂区之后的流动形态。随着 r_{1D} 和 r_{2D} 的增加,压力波在过渡区传播的时间变长,过渡区和过渡区向原油区转移阶段流态变化时间滞后,但过渡段极值几乎没有变化,压力导数曲线在过渡区向原油区转移阶段表现为向右平移。井底压差随 r_{1D} 和 r_{2D} 的增加而减小,说明CO₂与原油之间相互作用越充分越有利于后续CO₂的注入。

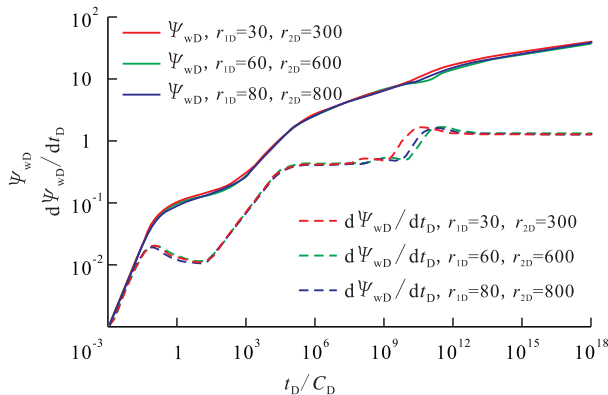


图5 r_{1D} 与 r_{2D} 对压力动态的影响

Fig.5 Effect of r_{1D} and r_{2D} on pressure dynamics

2.2.4 无因次井筒储集系数

设置不变参数值分别为: $S=1, Z_{wD}=0.5, M_{12}=1, M_{23}=3, \omega_{12}=2, \omega_{13}=3, L_{1D}=1, r_{1D}=30, r_{2D}=300, x_D=0.732$ 。

无因次井筒储集系数分别为 $10^{-4}, 10^{-5}$ 和 10^{-6} ,绘制试井曲线。由无因次井筒储集系数对压力动态的影响(图6)可见,无因次井筒储集系数越大,井筒储集时间越长,压力导数曲线第1个凸形极值越大,在第4阶段之后压力导数曲线出现左移,表明CO₂区线性流动阶段之后,所有流动状态出现时间提前。

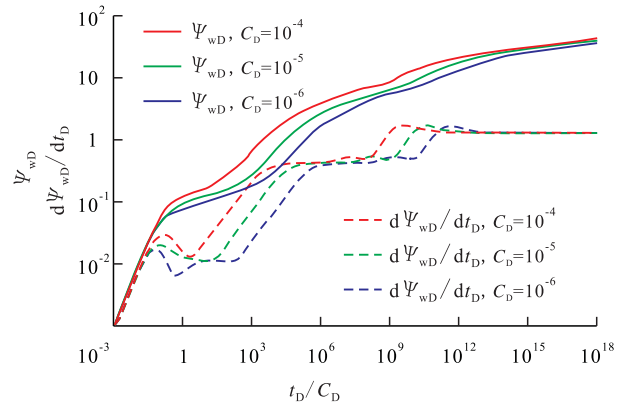


图6 无因次井筒储集系数对压力动态的影响

Fig.6 Effect of the non-dimensional wellbore storage coefficient on pressure dynamics

2.2.5 表皮系数

设置不变参数值分别为: $C_D=0.000\ 01, Z_{wD}=0.5, M_{12}=1, M_{23}=3, \omega_{12}=2, \omega_{13}=3, L_{1D}=1, r_{1D}=30, r_{2D}=300, x_D=0.732$ 。

表皮系数主要影响表皮流动阶段,分别设置为0.1, 0.5和1,由表皮系数对压力动态的影响(图7)可见,表皮系数越大,压力越大,其压力导数曲线的驼峰也越高。井污染越严重,井筒周围的阻力使表皮效应阶段持续时间增加,从而使气流流入井筒的难度增大。因此,在开发过程中,减少井筒污染有利于CO₂驱油。

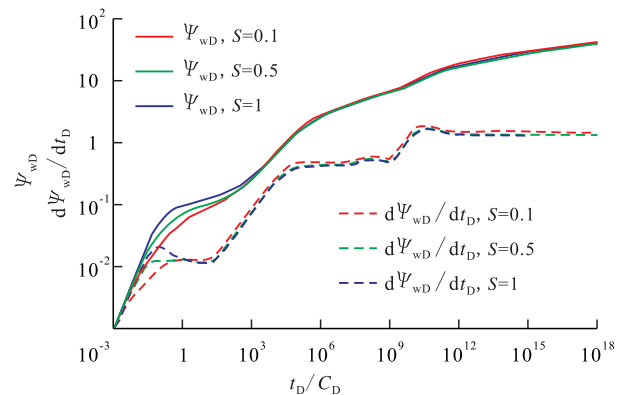


图7 表皮系数对压力动态的影响

Fig.7 Effects of epidermal factors on pressure dynamics

3 结论

推导了CO₂驱三区复合水平井模型,并分析了

试井曲线。通过采用拉普拉斯变换、正交变换和数值反演等一系列数学物理方法,求解出CO₂驱三区复合水平井模型的解析解。将试井曲线分为9个阶段,包括井筒储集阶段、表皮效应阶段、早期径向流阶段、线性流阶段、CO₂区平面径向流阶段、CO₂区向过渡区转移阶段、过渡区径向流阶段、过渡区向原油区转移阶段和原油区径向流阶段。

储容系数增加,压力导数曲线在CO₂区过渡阶段表现为向上移动,过渡区向原油区转移阶段时间提前;随着流体流度比增大,过渡区的极值增加;无因次井筒储集系数越大,第一极值越大,井筒储集时间越长,压力及其导数曲线表现为左移;表皮系数越大,压力曲线越高,压力导数曲线的第一极值越高。CO₂区半径和过渡区半径越大,其压力波在过渡区传播的时间就越长,过渡区和原油区的过渡段流态变化时间滞后,压力导数曲线表现为向右平移,其注入压力减小,有利于后续CO₂的注入。

符号解释:

r ——径向距离, m; 下标 D——无因次; L ——水平截面长度, m; t ——时间, h; η ——渗透系数; 下标 1, 2, 3——CO₂区、过渡区、原油区; K_h ——水平渗透率, D; ϕ ——孔隙度, %; μ_g ——地层气体粘度, mPa·s; C_g ——气体井筒储集系数; q ——产油量, m³/d; q_{sc} ——地面产油量, 10⁴ m³/d; h ——储层厚度, m; p_i ——初始压力, MPa; p ——压力, MPa; 下标 sc——标准状态; T ——温度, K; Z ——压缩因子; Ψ ——压力, MPa; m ——视压力, MPa²/(mPa·s); i ——1, 2, 3, …; C ——井筒储集系数, m³/MPa; C_l ——系统总压缩系数, MPa⁻¹; M_{12} ——CO₂区与过渡区流度比; K_{rg} ——气的相对渗透率; K_{ro} ——油的相对渗透率; μ_o ——地层原油粘度, mPa·s; M_{23} ——过渡区与原油区流度比; ω_{12} ——CO₂区与过渡区储容系数之比; ω_{13} ——CO₂区与原油区储容系数之比; K_v ——垂直渗透率, D; z ——垂直距离, m; ε ——微小变量; z_w ——水平截面位置, m; Ψ_D ——无因次压力; Ψ_{wD} ——无因次井底压力; s ——拉普拉斯变换系数; 上标“-”——拉普拉斯变换域; 上标“=”——正交变换域; n ——变量, $n=0, 1, 2, \dots$; I_0 ——零阶第一类虚宗量 Bessel 函数; K_0 ——零阶第二类虚宗量 Bessel 函数; K_1 ——一阶第二类虚宗量 Bessel 函数; x ——横坐标值, m; $\bar{\xi}_{wD0}$ ——变形函数; C_0 ——常数; C_n ——变量, $n=0, 1, 2, \dots$; $\bar{\psi}_{wD0}$ ——拉普拉斯域下无因次初始井底压力; x_{wD} ——无因次井底 x 轴距离, m; y_D ——无因次径向 y 轴距离, m; y_{wD} ——无因次井底 y 轴距离, m; S ——表皮系数; $\bar{\psi}_{wD}$ ——拉普拉斯域下无因次井底压力。

参考文献:

[1] 曹学良, 郭平, 杨学峰, 等. 低渗透油藏注气提高采收率前景分析[J]. 天然气工业, 2006, 26(3): 100-102.

- CAO Xueliang, GUO Ping, YANG Xuefeng, et al. An analysis of prospect of EOR by gas injection in low-permeability oil reservoir [J]. Natural Gas Industry, 2006, 26(3): 100-102.
- [2] 程杰成, 刘春林, 汪艳勇, 等. 特低渗透油藏二氧化碳混相驱试验研究[J]. 特种油气藏, 2016, 23(6): 64-67.
- CHENG Jiecheng, LIU Chunlin, WANG Yanyong, et al. Near-miscible CO₂ flooding test in ultra-low permeability oil reservoir [J]. Special Oil & Gas Reservoirs, 2016, 23(6): 64-67.
- [3] SU Kun, LIAO Xinwei, ZHAO Xiaoliang. Transient pressure analysis and interpretation for analytical composite model of CO₂ flooding [J]. Journal of Petroleum Science and Engineering, 2015, 125: 128-135.
- [4] AFIDICK D, KACZOROWSKI N J, BETTE S. Production performance of a retrograde gas reservoir: A case study of the Arun Field [R]. SPE 28749, 1994.
- [5] 崔传智, 吴忠维, 杨勇, 等. 缝洞型碳酸盐岩油藏压裂直井非稳态复合产能模型[J]. 油气地质与采收率, 2018, 25(1): 61-67.
- CUI Chuanzhi, WU Zhongwei, YANG Yong, et al. Unsteady compound productivity model of fractured vertical well in fractured-vuggy carbonate reservoirs [J]. Petroleum Geology and Recovery Efficiency, 2018, 25(1): 61-67.
- [6] 苏玉亮, 孟凡坤, 周诗雨, 等. 低渗透油藏CO₂驱试井曲线特征分析[J]. 科技导报, 2015, 33(18): 34-39.
- SU Yuliang, MENG Fankun, ZHOU Shiyu, et al. Characteristics analysis of well testing curve of CO₂ flooding in low permeability reservoir [J]. Science & Technology Review, 2015, 33(18): 34-39.
- [7] RAHIMZADEH Alireza, BAZARGAN Mohammad, DARVISHI Rouhollah, et al. Condensate blockage study in gas condensate reservoir [J]. Journal of Natural Gas Science and Engineering, 2016, 33: 634-643.
- [8] 李友全, 孟凡坤, 阎燕, 等. 考虑流体非均质性的低渗透油藏CO₂驱试井分析[J]. 岩性油气藏, 2016, 28(4): 106-112.
- LI Youquan, MENG Fankun, YAN Yan, et al. Pressure transient analysis on CO₂ flooding in low permeability reservoirs considering fluid heterogeneity [J]. Lithologic Reservoirs, 2016, 28(4): 106-112.
- [9] 侯彬彬, 卢德唐, 李道伦. 考虑热效应的CO₂气井试井压力模型和计算方法[J]. 中国科学技术大学学报, 2011, 41(3): 227-232.
- HOU Binbin, LU Detang, LI Daolun. Pressure model and calculation of well test for gas wells with CO₂ injection considering thermal effect [J]. Journal of University of Science and Technology of China, 2011, 41(3): 227-232.
- [10] ZHU Yin Hai, WANG Zhecheng, YANG Yiping, et al. Flow visualization of supersonic two-phase transcritical flow of CO₂ in an ejector of a refrigeration system [J]. International Journal of Refrigeration, 2017, 74(3): 352-359.
- [11] 伦增珉, 王锐, 吕成远, 等. 低渗透油藏二氧化碳驱修正毛管数理论及参数优化[J]. 油气地质与采收率, 2016, 23(2): 83-86, 92.
- LUN Zengmin, WANG Rui, LÜ Chengyuan, et al. Study on modified capillary number theory and its application in parameter opti-

- mization of CO₂ flooding in low permeability reservoirs [J]. *Petroleum Geology and Recovery Efficiency*, 2016, 23(2): 83-86, 92.
- [12] TANG R W, AMBASTHA A K. Analysis of CO₂ pressure transient data with two- and three-region analytical radial composite models [R]. *SPE* 18275, 1988.
- [13] AMBASTHA A K, RAMEY Jr H R. Pressure transient analysis for a three-region [R]. *SPE* 24378, 1992.
- [14] 郝宏达, 侯吉瑞, 赵凤兰, 等. 低渗透非均质油藏二氧化碳非混相驱窜逸控制实验 [J]. *油气地质与采收率*, 2016, 23(3): 95-100.
- HAO Hongda, HOU Jirui, ZHAO Fenglan, et al. Experiments of gas channeling control during CO₂ immiscible flooding in low permeability reservoirs with heterogeneity [J]. *Petroleum Geology and Recovery Efficiency*, 2016, 23(3): 95-100.
- [15] 章星, 韩磊, 周栋华, 等. CO₂ 细管驱油实验混相动态特征表征方法 [J]. *大庆石油地质与开发*, 2018, 37(1): 122-127.
- ZHANG Xing, HAN Lei, ZHOU Donghua, et al. Characterizing method of the dynamic characteristics of CO₂ slim-tube miscible oil flooding test [J]. *Petroleum Geology & Oilfield Development in Daqing*, 2018, 37(1): 122-127.
- [16] 吕成远, 王锐, 赵淑霞, 等. 低渗透油藏 CO₂ 非混相驱替特征曲线研究 [J]. *油气地质与采收率*, 2017, 24(5): 111-114.
- LÜ Chengyuan, WANG Rui, ZHAO Shuxia, et al. Study on displacement characteristic curve in CO₂ immiscible flooding for low permeability reservoirs [J]. *Petroleum Geology and Recovery Efficiency*, 2017, 24(5): 111-114.
- [17] LI Xiaoping, CAO Lina, LUO Cheng, et al. Characteristics of transient production rate performance of horizontal well [J]. *Journal of Petroleum Science and Engineering*, 2017, 125(158): 92-106.
- [18] CELIS V, SILVA R, RAMONES M, et al. A new model for pressure [J]. *SPEJ*, 1994, 2(1): 126-135.
- [19] 朱建伟, 邵长金, 廖新维, 等. 注二氧化碳混相驱试井模型及压力分析 [J]. *油气井测试*, 2011, 20(4): 1-4.
- ZHU Jianwei, SHAO Changjin, LIAO Xinwei, et al. Miscible flooding well test model with carbon dioxide injection and its pressure analysis [J]. *Well Testing*, 2011, 20(4): 1-4.
- [20] 章星, 王珍珍, 王帅, 等. 可视装置中 CO₂ 与正戊烷或原油接触特征和表征方法 [J]. *石油实验地质*, 2017, 39(3): 402-408.
- ZHANG Xing, WANG Zhenzhen, WANG Shuai, et al. Visual contact characteristics and characterization of the CO₂ and n-pentane/crude oil interface [J]. *Petroleum Geology & Experiment*, 2017, 39(3): 402-408.
- [21] JONES J R, RAGHAVAN R. Interpretation of flowing well responses in gas condensate wells [J]. *SPE Formation Evaluation*, 1988, 3(3): 578-594.
- [22] 宋考平, 祝俊峰, 刘泽俊, 等. 多区复合油藏非牛顿幂律流体试井解释 [J]. *石油学报*, 1997, 18(2): 78-83.
- SONG Kaoping, ZHU Junfeng, LIU Zejun, et al. Well test analysis for a compound reservoir with non-Newtonian power law fluids flow [J]. *Acta Petrolei Sinica*, 1997, 18(2): 78-83.

编辑 刘北羿

《中外能源》杂志征订启事

《中外能源》杂志创刊于1996年,月刊,国内外公开发行,国内刊号CN 11-5438/TK,国际刊号ISSN 1673-579X,大16开,每期定价18元,全年定价216元。邮发代号:80-674

《中外能源》杂志主要立足能源领域,特别是石油、天然气、煤炭及新能源和可再生能源领域,重点围绕能源战略规划和建设、新技术开发和应用、节能与清洁生产技术及其产业化应用等热点问题报道。主要栏目包括:能源战略与政策研究、替代能源与新能源、油气勘探与开发、炼油与化工技术、节能与环境保护、区域能源、寰球能源动态等。

《中外能源》杂志系美国《化学文摘》(CA)、美国《石油文摘》(PA)、美国《剑桥科学文摘》(CSA)、美国《乌利希期刊指南》、波兰《哥白尼索引》(IC)、中国期刊网、中国期刊全文数据库、中国核心期刊(遴选)数据库收录期刊。

欢迎广大读者订阅。

银行电汇:《中外能源》杂志社 开户银行:建行北京地坛支行 账号:11001042900053003411

电话:010-64294880 传真:010-64295078 电子邮箱:zhongwny@163.com